



# Photocatalytic degradation of gaseous pollutants on nanostructured TiO<sub>2</sub> films of various thickness and surface area

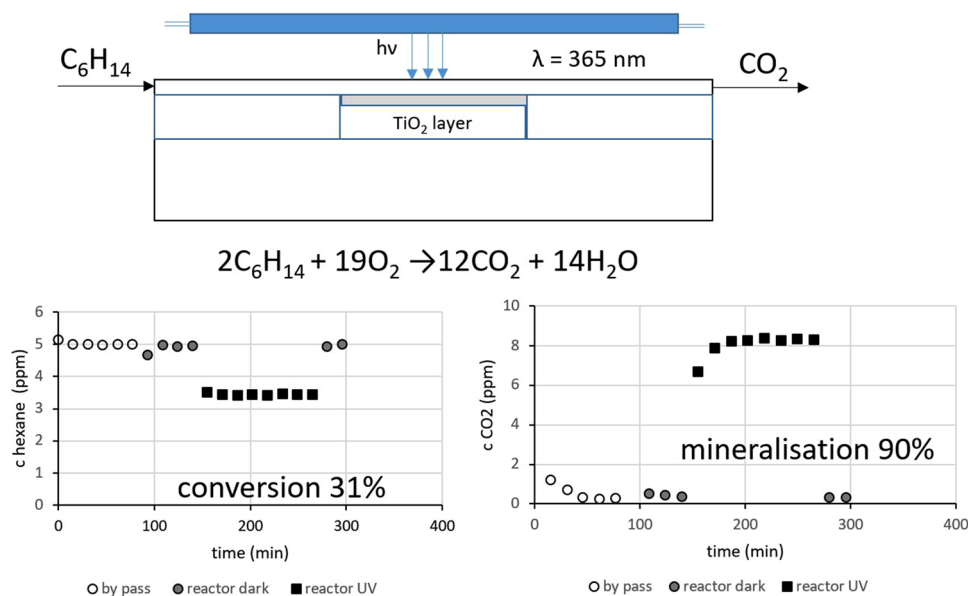
Michal Baudys<sup>1</sup> · Eleonore Berthet<sup>1</sup> · Jan M. Macak<sup>2,3</sup> · Miloslav Lhotka<sup>1</sup> · Josef Krýsa<sup>1</sup>

Received: 1 September 2022 / Accepted: 23 December 2022 / Published online: 6 February 2023  
© The Author(s) 2023

## Abstract

This work deals with the preparation of TiO<sub>2</sub> nanoparticulate layers of various mass (0.05 mg/cm<sup>2</sup> to 2 mg/cm<sup>2</sup>) from three commercial nanopowder materials, P90, P25 and CG 300, their characterisation (profilometry, BET and SEM) and evaluation of their photocatalytic activity in the gaseous phase in a flow-through photoreactor according to the ISO standard (ISO 22197-2). Hexane was chosen as a single model pollutant and a mixture of four compounds, namely acetaldehyde, acetone, heptane and toluene was used for the evaluation of the efficiency of simultaneous removal of several pollutants. A linear dependence between the layer mass and the layer thickness for all materials was found. Up to a layer mass 0.5 mg/cm<sup>2</sup>, the immobilisation P90 and P25 powder did not result in a decrease in BET surface area, whereas with an increase in layer mass to 1 mg/cm<sup>2</sup>, a decrease of the BET surface was observed, being more significant in the case of P90. The photocatalytic conversion of hexane was comparable for all immobilised powders up to a layer mass of 0.5 mg/cm<sup>2</sup>. For higher layer mass, the photocatalytic conversion of hexane on P25 and P90 differ; the latter achieved about 30% higher conversion. In the case of the simultaneous degradation of four compounds, acetaldehyde was degraded best, followed by acetone and toluene; the least degraded compound was heptane. The measurement of released CO<sub>2</sub> revealed that 90% of degraded hexane was mineralised to CO<sub>2</sub> and water while for a mixture of 4 VOCs, the level of mineralisation was 83%.

## Graphical abstract



**Keywords** TiO<sub>2</sub> · Nanoparticulate films · P90 · P25 · Photocatalysis · ISO 22197-2 · Gaseous pollutants

Extended author information available on the last page of the article

## 1 Introduction

Semiconductor photocatalysis on TiO<sub>2</sub> surfaces represents a promising method for the atmospheric decomposition of volatile organic compounds (VOCs), such as formaldehyde or acetaldehyde [1]. Such compounds can be released from building materials in interior environment, causing non-specific diseases including respiratory irritation symptoms, headaches, dizziness, and fatigue. Such non-specific symptoms are generally marked as sick building syndrome [2]. Various photocatalytic technologies, including air purifiers [3] or photocatalytic paints [4–6], prepared with the aim of improving interior air quality, appear nowadays on the market. The photoactive layers in these products are based on TiO<sub>2</sub> nanoparticles and their compacted networks. The photocatalytic efficiency of P25 is often determined using the removal of NO<sub>x</sub> (ISO 22197-1), as an example of a typical outdoor pollutant [7, 8] or acetaldehyde [9, 10], as an example of a typical indoor pollutant. Another model pollutant can be hexane [11], whose higher number of carbon atoms makes it easier to measure the amount of mineralization (formation of CO<sub>2</sub>).

Commercial TiO<sub>2</sub> powder photocatalysts, such as Aeroxide P25 [12], produced by Evonik, are often studied materials in environmental photocatalytic processes, but for practical application of photocatalytic air treatment, it is important to immobilise photocatalyst powders in the form of thin layers using dip-coating [13], electrophoresis [14], doctor blading or drop casting [15, 16].

There are several studies focused on the removal of volatile organic compounds (VOCs), with attention paid to the reaction mechanism [17–19], reactor design [20, 21], effect of process parameters such as flow rate, UV intensity [22, 23], humidity [24, 25] or large scale studies including photocatalytic de-polluting efficiency in indoor car parks [26] or simulated street canyons [27]. For the determination of photocatalytic activity in the gaseous phase, acetaldehyde is often used as a model compound [28–31]. Acetaldehyde is degraded more easily compared to toluene [32] and is also used as model pollutant in the ISO standard (ISO 22197-2). Beside acetaldehyde, hexane is also used especially in the case where CO<sub>2</sub> formation is simultaneously measured [11].

The effect of layer thickness and surface area on the rate of photocatalytic oxidation of organic compounds was predominantly studied in the liquid phase. Krýsa et al. [15] studied the influence of the thickness of TiO<sub>2</sub> P25 films on photocurrent and degradation rate of oxalic acid. It was found that the optimal thickness of the film was about 0.5 μm, with further increase of the thickness leading to a photocurrent decrease. Jung et al. [33] studied the influence of TiO<sub>2</sub> layer thickness prepared by chemical vapour

deposition (CVD) on the degradation rate of methylene blue. The degradation rate increased up to 3 microns, but further increase in layer thickness had no influence on the degradation rate. Another study showed the influence of surface area of TiO<sub>2</sub> on the degradation rate of oxalic acid [34]. Although TiO<sub>2</sub> materials exhibited much higher surface area than P25 (about 300 m<sup>2</sup>/g), the photocatalytic activity reached only 60% of that of TiO<sub>2</sub> P25 which was explained by more efficient charge recombination in smaller particles of TiO<sub>2</sub> in comparison with bigger particles of P25. Concerning the gaseous phase, in our recent work [35], we described the influence of the thickness of TiO<sub>2</sub> nanotubes on the photocatalytic efficiency of hexane and benzene removal. It was found that the photocatalytic efficiency increased with increasing layer thickness from 0.17 to 14 μm. In the case of hexane, there was no sign of deactivation but in the case of benzene the initial conversion degree decreased [35].

In practical applications, we usually have not only one single compound but a mixture of various types of compounds. Stucchi et al. [36] described the photocatalytic performance of TiO<sub>2</sub> material during simultaneous degradation of 17 compounds including aldehydes, hydrocarbons and chlorinated compounds. The authors observed that VOCs compete for the adsorption on TiO<sub>2</sub> surface according to their polarity. Thus, the degradation reaction was slower compared to that of a single compound. Acetaldehyde and formaldehyde when used as single pollutants were photocatalytically degraded with a conversion degree of almost 100%; on the other hand, when they were in a mixture, the conversion degree of each pollutant dropped significantly.

Even though TiO<sub>2</sub> P25 is often deposited on a glass support using drop casting [16, 37], the main attention is paid to the texture properties of pure powder, and the textural properties of layers themselves are often neglected. Thus, the objective of this work was to evaluate the photocatalytic activity of nanoparticulate layers prepared from several commercial TiO<sub>2</sub> powder photocatalysts with special emphasis on the detailed characterization (layer mass, layer thickness, porosity, textural properties). The photocatalytic activity in the gaseous phase was determined using the standard ISO setup ((ISO-22197-2) with a single pollutant (hexane) and a mixture of four pollutants (acetaldehyde, heptane, acetone and toluene), and special attention was given to the evaluation of the level of mineralization.

## 2 Experimental

### 2.1 Preparation and characterization of TiO<sub>2</sub> nanoparticulate layers

Soda lime glass slides (5 × 10 × 0.3 cm) were used as support. Support cleaning involved a sequence of washing steps in an ultrasonic bath [DT100H (Bandelin electronic GmbH & Co. KG, frequency 35 kHz)] using acetone, ethanol, and water. Layers were prepared by drop-casting. First, the appropriate amount of the photocatalyst was dispersed in 50 ml water using treatment in ultrasonic bath for 10 min. Afterwards, 10 ml of the prepared suspension was deposited on the glass supports and left to dry at room temperature.

X-ray diffraction (XRD) was performed with an X'Pert<sup>3</sup> MRD system (Malvern Panalytical). The thickness of the TiO<sub>2</sub> layer was determined using a profilometer (DektakXT, Bruker). The porosity of the TiO<sub>2</sub> layer ( $P$ , in %) was calculated as in our previous work [38], using the formula below (Eq. 1) where  $d$  is the layer thickness (cm),  $m_{\text{layer}}/S$  is the layer mass (mg/cm<sup>2</sup>),  $\rho_{\text{TiO}_2}$  represents the density of TiO<sub>2</sub> (g/cm<sup>3</sup>) and  $S$  is the geometrical surface area of the layer.

$$P = \frac{V_{\text{air}}}{V_{\text{layer}}} 100 = \frac{V_{\text{layer}} - V_{\text{TiO}_2}}{V_{\text{layer}}} 100 = \frac{\left(d - \frac{m_{\text{layer}}}{1000 \cdot S \cdot \rho_{\text{TiO}_2}}\right)}{d} 100. \quad (1)$$

Structural analysis was carried out using a Brunauer–Emmett–Teller (BET) concept. The specific surface area ( $S_{\text{BET}}$ ) was measured using the nitrogen (purity 5 N) sorption method (TriFlex, Micromeritics, USA) and the krypton (purity 4 N) sorption method (ASAP 2020, Micromeritics, USA). The samples were degassed at 200 °C for 12 h prior to measurement. The equilibration time in between the measurement steps was 20 s.

### 2.2 Determination of photocatalytic activity of TiO<sub>2</sub> nanoparticulate layers

Photocatalytic activity was determined using conditions based on ISO 22197-2 (removal of acetaldehyde). Instead of acetaldehyde, either hexane as a single pollutant (inlet

concentration 5 ppm), or a mixture of four pollutants (acetaldehyde, heptane, acetone and toluene, inlet concentration 1 ppm for each) was used. Conditions of individual photocatalytic tests in the gaseous phase are summarized in Table 1. A scheme of the whole apparatus for the measurement and the photoreactor, together with a corresponding description, are given in Figs. 1 and S1 (in Supplementary information), respectively. As a UV light source two UV A fluorescent tubes (Philips T8) with an emission maximum at 365 nm and an irradiance of 1 mW/cm<sup>2</sup> were used. The concentration of the model pollutants was determined using a gas chromatograph GC 7890B (Agilent) equipped with a flame-ionization detector (FID) and a methanizer (a chemical reactor that converts carbon dioxide and carbon monoxide to methane to enable sensitive detection by a FID (Jetanizer, Activated Research Company)).

The testing gas was prepared by mixing of synthetic air (AIR) with reactant gas from a calibration cylinder using two mass flow controllers (MFC). The gas to be reacted was either hexane (100 ppm) in nitrogen or a mixture of acetaldehyde, heptane, acetone and toluene (each 10 ppm) in nitrogen. Before mixing with calibration gas, synthetic air was divided in wet and dry flow lines, using two needle valves to control the relative humidity.

Photocatalytic activity was determined as follows. The concentration of the pollutant (e.g. hexane) in the testing gas was measured in regular intervals by GC using an FID. At first, the testing gas was introduced via 2 three valve vents (4) outside the photoreactor (bypass) and the concentration of the tested pollutant (e.g. hexane) was measured (GC with FID). After reaching a stable initial concentration of 5 ppm, the testing gas was introduced to the photoreactor in the dark (reactor dark) to see the potential adsorption of the tested pollutant on the TiO<sub>2</sub> surface (as a decrease in the concentration). Adsorption equilibrium was reached when the concentration returned back to 5 ppm. Then, the UV light was switched on (reactor light) and the output concentration of the tested pollutant (e.g. hexane) was measured. After a given time and reaching stable conversion of the tested pollutant the light was switched off (reactor dark). Tests with a mixture of 4 pollutants were performed in the

**Table 1** Conditions of photocatalytic experiments in the gaseous phase

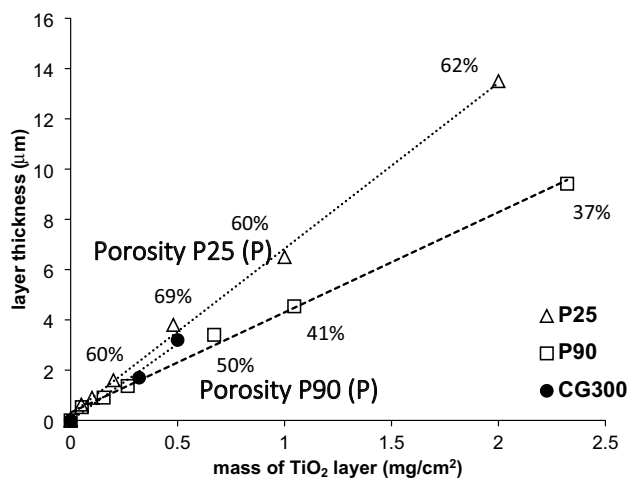
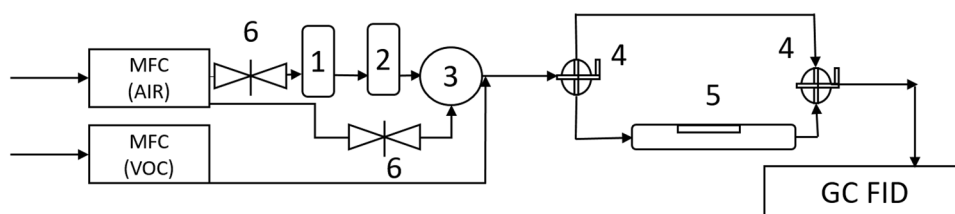
ISO test	ISO 22197–2 [39]	This study	
Model compound	Acetaldehyde	Hexane	Mixture of acetone, acetaldehyde, heptane and toluene
Initial concentration (ppm)	5	5	1 ppm per compound
Flowrate (dm <sup>3</sup> /min)	1	1	1
Relative humidity (%)	50	50	50
Irradiance of UV light (mW/cm <sup>2</sup> )	1	1	1

**Table 2** BET surface area and calculated roughness factor ( $R_f$ ) of P90 layers of different layer mass

Layer mass (mg/cm <sup>2</sup> )	Area of layer (cm <sup>2</sup> )	Mass of TiO <sub>2</sub> (mg)	Nitrogen		Krypton	
			$S_{\text{BET}}$ (m <sup>2</sup> /g)	$R_f$ (cm <sup>2</sup> /cm <sup>2</sup> )	$S_{\text{BET}}$ (m <sup>2</sup> /g)	$R_f$ (cm <sup>2</sup> /cm <sup>2</sup> )
0.2	11	2.2	132	264	111	222
0.5	10	5.0	116	580	110	550
1	11.2	11.2	79	790	66	660

**Table 3** BET surface area and calculated roughness factor ( $R_f$ ) of P25 layers of different layer mass

Layer mass (mg/cm <sup>2</sup> )	Area of layer (cm <sup>2</sup> )	Mass of TiO <sub>2</sub> (mg)	Nitrogen		Krypton	
			$S_{\text{BET}}$ (m <sup>2</sup> /g)	$R_f$ (cm <sup>2</sup> /cm <sup>2</sup> )	$S_{\text{BET}}$ (m <sup>2</sup> /g)	$R_f$ (cm <sup>2</sup> /cm <sup>2</sup> )
0.2	10.5	2.1	58	116	47	94
0.5	12	6.4	42	210	45	225
0.7	10.5	7.5	47	330	47	329
1	11.4	10.2	38	340	35	313

**Fig. 1** Scheme of used photocatalytic ISO apparatus (1—humidifying flask, 2—empty flask, 3—humidity meter, 4—three valve vent, 5—ISO reactor). *MFC* mass flow controller, *GC FID* gas chromatograph with flame-ionization detector**Fig. 2** Dependence of the TiO<sub>2</sub> layer thickness on the layer mass for three types of TiO<sub>2</sub> powders immobilised by drop-casting on glass support

same way. The concentration of all four pollutants was measured by GC FID.

### 3 Results and discussion

#### 3.1 Characterisation of TiO<sub>2</sub> nanopowders and layers

Table S1 (supplementary information) summarises the measured composition and structural and textural properties of studied TiO<sub>2</sub> nanopowders using XRD and BET (nitrogen adsorption). X-ray diffraction patterns of studied TiO<sub>2</sub> powders are shown in Fig. S2 (in SI). Both powder materials, P90 and P25, exhibited adsorption isotherms of type V indicating mesoporous material with a BET surface area of 109 and 45 m<sup>2</sup>/g, respectively. The N<sub>2</sub> adsorption isotherms of TiO<sub>2</sub> powders are shown in Fig. S3. The CG300 powder had the highest BET surface area (300 m<sup>2</sup>/g). It contained only anatase and the crystal size was about 5 nm. P25 and P90 exhibit both phases, Ohtani et al. reported that typical crystalline composition of P25 was 78% anatase and 14% rutile, the remaining 8% corresponds to amorphous phase [12]. The crystal size of anatase was around 22 nm in P25 and 13 nm in P90. For all powder materials, the crystal size calculated from XRD corresponded to the BET surface area.

To better understand the homogeneity of the obtained TiO<sub>2</sub> films, photographs of TiO<sub>2</sub> layers of different layer mass prepared by drop-casting from P90 powder

suspensions are shown in Fig S4 (in SI). It can be concluded that layers prepared from P25 and P90 show sufficient adhesion to the glass support up to a layer mass of 2 mg/cm<sup>2</sup>. On the other hand, layers prepared from CG300 with a layer mass above 0.5 mg/cm<sup>2</sup> are not very adherent and already a simple manipulation resulted in particle loss from the surface. This can be explained by the fact that even C300 has a high BET surface area and the smallest crystal size from all materials (Fig. S2 and S3 in SI), it consists of much bigger agglomerates which were not broken even by sonification of aqueous suspension (used before drop-casting deposition).

Figure 2 (and Table S2 in SI) shows the dependence of layer thickness on the layer mass for all three types of immobilised powders. Typical profilometric trace of a step – glass/TiO<sub>2</sub>\_P25 layer is shown in Fig. S5 (in SI). With increasing layer mass, the layer thickness proportionally increases. For the same layer mass, the highest layer thickness was observed for the P25 layer and the lowest for the P90 layer. This can be explained by the value of the calculated porosity (Eq. 1), for P25 layers the porosity was 60–70% and for P90 layers it was 40–50%. CG300 layers had a porosity about 50%, which is close to that of P90. This indicates that layers fabricated from powders of higher BET surface area (P90 and CG300) are more compact (lower porosity) than layers fabricated from powders of lower BET surface area (P25).

The specific surface areas of TiO<sub>2</sub> layers were evaluated using N<sub>2</sub> and Kr isotherms. Frequently, N<sub>2</sub> is used as adsorbate. For low surface areas, however, more accurate values are usually obtained with Kr instead of N<sub>2</sub> [38] due to the lower vapour pressure of Kr at the adsorption measurement temperature of 77 K compared to N<sub>2</sub>. Another reason is the fact that the mass of layers exposed to the test gas in the adsorption measurement is very small (limited by the size of samples which can be placed in the measurement flask). The N<sub>2</sub> adsorption isotherms are shown in Figs. S6a and

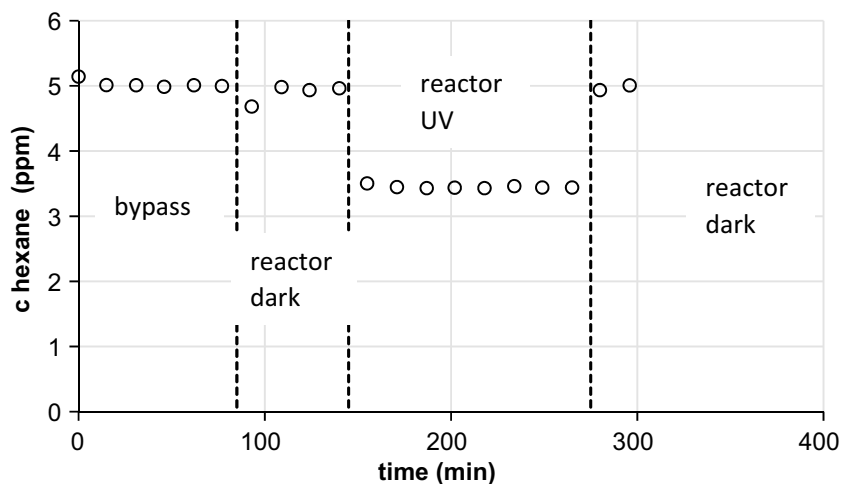
S7a and the Kr adsorption isotherms are shown in Figs. S6b and S7b. The specific surface areas per mass ( $S_{\text{BET}}$ ) and per geometrical area (dimensionless  $R_p$ ) of particulate layers of various layer mass are given in Tables 2 and 3, respectively.

It can be seen that the values of BET obtained by adsorption of either N<sub>2</sub> or Kr are very similar. Only for the smallest layer mass (0.2 mg/cm<sup>2</sup>), the BET value obtained from N<sub>2</sub> adsorption is much higher (about 20%) than that obtained from Kr adsorption. The reason is that the adsorbed amount of N<sub>2</sub> on glass (taken as reference) was about 10–20% of the adsorbed amount of N<sub>2</sub> on this small sample (see Figs. S6a and S7a). For layers of mass 0.2 and 0.5 mg/cm<sup>2</sup>, the observed value of BET surface area corresponds to the value observed for both powders. But for layer of mass 1 mg/cm<sup>2</sup>, the BET value is about 40% (P90) and 25% lower than that for powders. This was observed either using N<sub>2</sub> or Kr isotherm. The decrease in the BET value is more pronounced for P90 and this can be connected with the decrease in the calculated porosity of these layers from 50 to 41%.

### 3.2 Photocatalytic degradation of hexane as a single pollutant

It is important to mention that for the present implementation of the experiment, the conversion is governed by the length of the reactor, the flow rate and the irradiance. In the present study, these parameters are chosen according to the ISO standard (see Table 1). Fig S8 (in SI) shows a comparison of the photocatalytic activity of hexane and of acetaldehyde. It follows that acetaldehyde can be more easily removed (conversion about 75%). To prevent potential mass transfer limitation we used hexane instead of acetaldehyde, which is more difficult to be removed (conversion about 31%). The second reason for using hexane was the evaluation of the level of mineralization. Total mineralization of 1 mol of hexane results in the production of 6 mols

**Fig. 3** Concentration of hexane during a photocatalytic experiment





of CO<sub>2</sub> (while in the case of acetaldehyde only 2 mols of CO<sub>2</sub> are produced).

Figure 3 shows the concentration of hexane during the typical gas phase photocatalytic experiment on the P25 layer with the layer mass 0.5 mg/cm<sup>2</sup>. From each experiment, the hexane conversion was calculated as the difference between the hexane concentration in the dark (average from 3 subsequent concentrations before the light was switched on) and under light (average from 3 subsequent concentration measurements before the light was switched off).

The dependence of hexane conversion on the layer mass for all immobilised powders (P90, P25 and CG300) is shown in Fig. 4. The degradation experiments were repeated (three times) and each calculated conversion degree was found to be within ± 10% of the mean value. In the case of CG300, due to the poor adhesion to the glass substrate, only results for a layer mass up to 0.5 mg/cm<sup>2</sup> are shown. It can be seen that up to the layer mass of 0.5 mg/cm<sup>2</sup>, the hexane conversion degree for all three TiO<sub>2</sub> layers is comparable and gradually increases with increasing layer mass (layer thickness). With further increase of the layer mass, P25 and P90 layers behave differently. In case of P90, the conversion degree steeply increases up to 1 mg/cm<sup>2</sup> and then remains almost unchanged for layer masses of 2.1 and 2.3 mg/cm<sup>2</sup>. In the case of P25, the increase of the conversion degree is not as steep as for P90, but increases up to a layer mass of 1.5 mg/cm<sup>2</sup> and for the layer mass of 2 mg/cm<sup>2</sup> there is only a very small increase.

The increase in the layer mass (thickness) may have a positive influence on pollutant photocatalytic conversion due to i) increase in the amount of absorbed light and ii) increase of adsorption sites for substances present in the gas phase. Figure 4 shows that the conversion degree increases only up to layer mass ~ 1 mg/cm<sup>2</sup> (layer thickness 4–6 μm). This would mean that above this thickness (4–6 μm), either the UV light cannot reach the whole TiO<sub>2</sub> surface, or whole

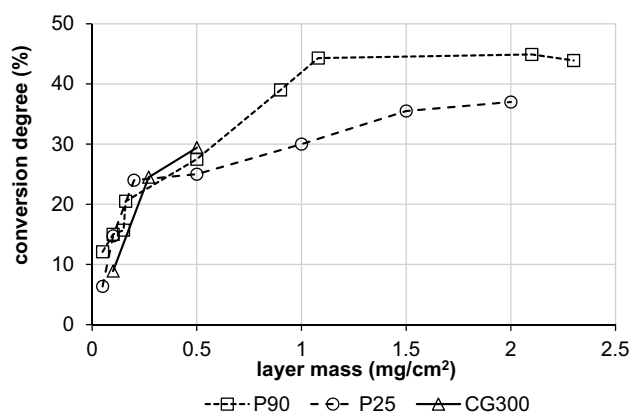


**Fig. 4** Conversion of hexane as a function of layer mass for layers prepared from P90, P25 and CG 300 powder

surface is not available for adsorption of hexane [40] or both. From the layer thickness measured by profilometry and calculated porosity (Eq. 1), an effective TiO<sub>2</sub> layer thickness was calculated and shown in Table S2 (in SI). Based on the work [41] for effective TiO<sub>2</sub> thickness 1 μm (layer mass of our layers ~ 0.4 mg cm<sup>2</sup>) more than 95% light is absorbed. The significant increase of conversion degree for layer mass 0–0.3 mg cm<sup>2</sup> is predominantly due to the increase in amount of absorbed light. The further slower increase of conversion degree for layer mass above 0.3 mg cm<sup>2</sup> can be explained by increasing the amount of adsorption sites.

From the comparison of P25 and P90 layers of the same layer mass, hexane conversion is about 10–30% higher on P90 layer than on P25 layers. The explanation can be in significantly higher value of BET for P90, but the increase in conversion is much smaller (10–30%) than the increase in the specific area (about 100%). A similar dependence of photocatalytic activity on layer mass (thickness) was reported in our previous work [42]. Up to a layer mass 0.4 mg/cm<sup>2</sup>, the photocatalytic degradation rate (of model ink 2,6-dichloroindophenol) increased proportionally with the layer mass. For a layer mass higher than 0.3 mg/cm<sup>2</sup>, there was no significant improvement of photocatalytic degradation rate (of oxalic acid) [15].

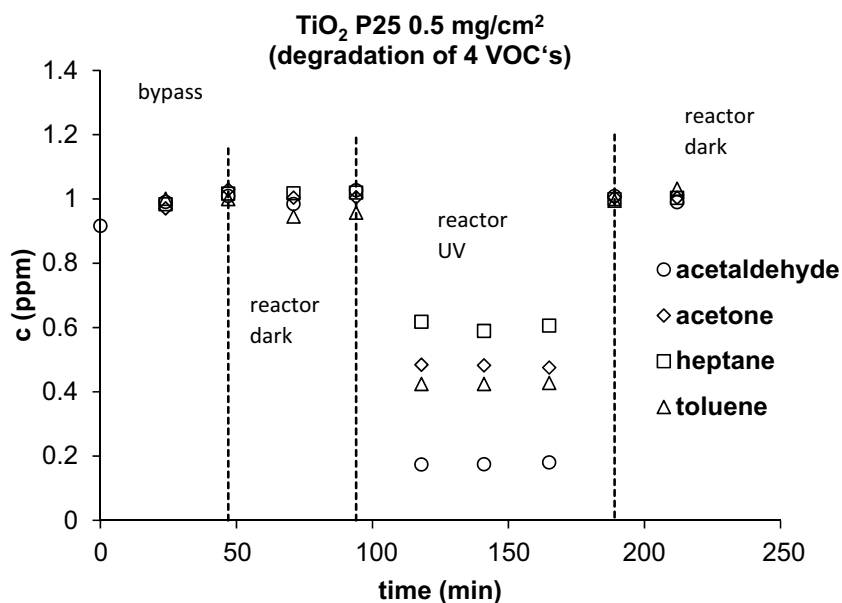
Fig. S9a and b (in SI) show the repeated removal of hexane on a layer consisting of P25. The conversion degree in two subsequent experiments did not decrease and was around 40%. A similar observation was made in the case of P90 and CG300. It suggests that during hexane degradation, there is no photocatalyst deactivation and photocatalytic treatment can be used repeatedly.

### 3.3 Simultaneous degradation of four pollutants

In a practical application of photocatalytic air treatment, there is not just one single pollutant, but there is always a mixture of various organics pollutant. Thus in the next step, instead of the single pollutant hexane we used a mixture of four organic pollutants, i.e. acetaldehyde, acetone, heptane, and toluene. The conditions (flow rate, relative humidity) were the same as for hexane, but the inlet concentration of each compound was lower (1 ppm), so that the total concentration was 4 ppm (value close to 5 ppm of the single pollutant hexane).

Figure 5 shows the concentration of 4 VOC's during the typical gas phase photocatalytic experiment on the P25 layer with the layer mass 0.5 mg/cm<sup>2</sup>. Other experiments with longer UV illumination (210 min.) showed that the conversion of all pollutants remained constant without any sign of photocatalyst deactivation. Acetaldehyde exhibited the highest degradation rate, followed by acetone and toluene that were degraded with a similar efficiency, while heptane had the lowest degradation rate. A similar trend was reported

**Fig. 5** Concentration of four VOC's during a photocatalytic experiment on P25 layer ( $0.5 \text{ mg/cm}^2$ )



in [43] where authors used a standard method (French XP B44-013, ISO 18560-1:2014) for the evaluation of the photocatalytic efficiency of VOC removal in a closed chamber. In another work, it was shown that oxygen containing compounds such as alcohols and ketones were more easily degraded than alkanes [22]. It seems that the difference in photocatalytic conversion degrees of individual compounds correlate with their solubility in water. Acetaldehyde is miscible with water but the solubility of heptane is very small ( $3.4 \text{ mg/l H}_2\text{O}$ ) [44]. The much higher rate of photocatalytical oxidation of acetaldehyde can be thus explained by the higher affinity to the hydrophilic surface of irradiated  $\text{TiO}_2$ .

Figure S10 shows the comparison of acetaldehyde, acetone, heptane and toluene conversion on particulate layers of three commercial  $\text{TiO}_2$  powders with a layer mass of  $0.5 \text{ mg/cm}^2$ . The preference in degradation of an individual pollutant did not depend on the type of  $\text{TiO}_2$  powder. Acetaldehyde was the easiest, whereas heptane was the most difficult to be oxidatively removed.

### 3.4 Mineralization and production of $\text{CO}_2$

Figure 6a shows the evolution of  $\text{CO}_2$  produced by the photocatalytic decomposition of hexane. According to the molar ratio of hexane/ $\text{CO}_2$ , the totally oxidized hexane (initial concentration  $5 \text{ ppm}$ ) produces  $30 \text{ ppm}$  of  $\text{CO}_2$ . In the present case, the conversion is only about 31% so the theoretical amount of  $\text{CO}_2$  produced corresponds to  $9.3 \text{ ppm}$ . Our measured value of produced  $\text{CO}_2$  was about  $8.4 \text{ ppm}$  indicating that about 90% of degraded hexane was transformed to  $\text{CO}_2$  and the production of organic intermediates was very small. A similar fraction of mineralization leading to  $\text{CO}_2$  (about 98%) was observed for  $\text{TiO}_2$ , while in the case of  $\text{ZnO}$ , the

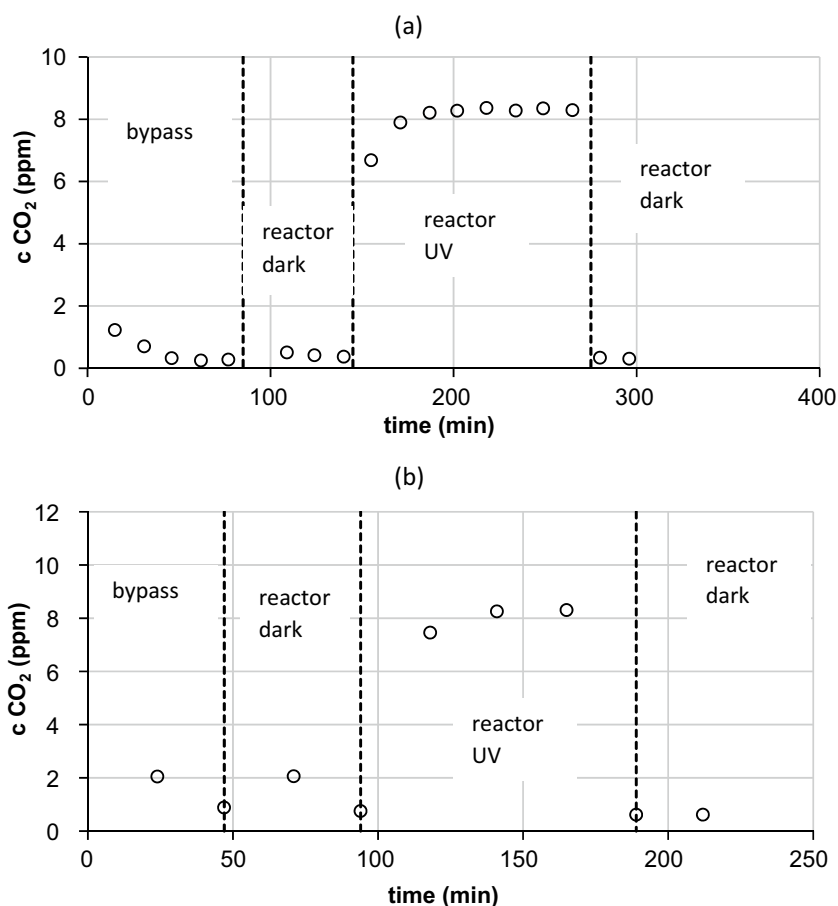
value was lower (about 57%) and a number of oxygen containing intermediates (3-hexanone, 2-hexanone, 3-hexanol and 2-hexanol) was identified [45]. Figure 6b shows the evolution of  $\text{CO}_2$  produced by the photocatalytic decomposition of 4 VOCs. The theoretical amount of produced  $\text{CO}_2$ , which was calculated from measured conversion degrees of acetaldehyde (82%), acetone (50%), heptane (40%) and toluene (56%) was  $10 \text{ ppm}$ . As follows from Fig. 6b, the measured concentration of  $\text{CO}_2$  was about  $8.3 \text{ ppm}$  indicating that 83% of degraded pollutants were transformed to  $\text{CO}_2$  and thus mineralised.

## 4 Conclusion

Texture properties of  $\text{TiO}_2$  layers with layer mass up to  $2 \text{ mg/cm}^2$  prepared from aqueous suspensions of three commercial  $\text{TiO}_2$  powders (P25, P90, and CG300) by drop-casting techniques were investigated. Good agreement of determined BET surface area for powder and layers was observed for P90 and P25 up to layer mass  $0.5 \text{ mg/cm}^2$  (proved by measuring of  $\text{N}_2$  and Kr isotherms) indicating that the powder immobilisation does not result in a decrease in real surface area. With an increase in layer mass to  $1 \text{ mg/cm}^2$ , a decrease of BET surface area was observed, which was more significant in the case of P90.

It was found that for layers with the mass up to  $0.5 \text{ mg/cm}^2$ , the photocatalytic conversion of hexane was comparable for all immobilised powders. With increasing layer mass photocatalytic conversion of hexane on P25 and P90 differ; the latter catalyst achieved an about 30% higher conversion degree. In the case of simultaneous photocatalytic decomposition of four VOCs (acetaldehyde, acetone, toluene and

**Fig. 6** Concentration of CO<sub>2</sub> produced by the decomposition of hexane a) (inlet concentration 5 ppm) and concentration of CO<sub>2</sub> produced by the decomposition of 4 VOCs (the inlet concentration of each VOC was 1 ppm)



heptane), acetaldehyde exhibited the highest conversion degree which can be explained by the highest water solubility and thus the highest affinity to the hydrophilic TiO<sub>2</sub> surface. The measurement of released CO<sub>2</sub> by photocatalytic oxidation of pollutants revealed that 90% of degraded hexane was mineralised to CO<sub>2</sub> and water while for a mixture of four VOCs the level of mineralisation was 83%.

**Supplementary Information** The online version contains supplementary material available at <https://doi.org/10.1007/s43630-022-00359-0>.

**Acknowledgements** The authors acknowledge the Czech Science Foundation (project 21-27243S) for the financial support.

**Funding** Open access publishing supported by the National Technical Library in Prague.

**Data availability** Data will be available on the request.

**Open Access** This article is licensed under a Creative Commons Attribution 4.0 International License, which permits use, sharing, adaptation, distribution and reproduction in any medium or format, as long as you give appropriate credit to the original author(s) and the source, provide a link to the Creative Commons licence, and indicate if changes were made. The images or other third party material in this article are included in the article's Creative Commons licence, unless indicated otherwise in a credit line to the material. If material is not included in the article's Creative Commons licence and your intended use is not

permitted by statutory regulation or exceeds the permitted use, you will need to obtain permission directly from the copyright holder. To view a copy of this licence, visit <http://creativecommons.org/licenses/by/4.0/>.

## References

- Paz, Y. (2010). Application of TiO<sub>2</sub> photocatalysis for air treatment: Patents' overview. *Applied Catalysis B: Environmental*, *99*, 448–460.
- Redlich, C. A., Sparer, J., & Cullen, M. R. (1997). Sick-building syndrome. *The Lancet*, *349*, 1013–1016.
- Zhong, L., & Haghghat, F. (2015). Photocatalytic air cleaners and materials technologies—Abilities and limitations. *Building and Environment*, *91*, 191–203.
- Ângelo, J., Andrade, L., & Mendes, A. (2014). Highly active photocatalytic paint for NO<sub>x</sub> abatement under real-outdoor conditions. *Applied Catalysis A: General*, *484*, 17–25.
- Salthammer, T., & Fuhrmann, F. (2007). Photocatalytic surface reactions on indoor wall paint. *Environmental Science & Technology*, *41*, 6573–6578.
- Mills, A., & Elouali, S. (2015). The nitric oxide ISO photocatalytic reactor system: Measurement of NO<sub>x</sub> removal activity and capacity. *Journal of Photochemistry and Photobiology A: Chemistry*, *305*, 29–36.
- Baudys, M., Andrews, R., Han, R., O'Rourke, C., Hodgen, S., Krysa, J., & Mills, A. (2021). Photocatalytic paints for NO<sub>x</sub>



- removal: Influence of various weathering conditions. *Journal of Environmental Chemical Engineering*, 9, 106172.
8. Mills, A., Hill, C., & Robertson, P. K. J. (2012). Overview of the current ISO tests for photocatalytic materials. *Journal of Photochemistry and Photobiology A: Chemistry*, 237, 7–23.
  9. Han, R., Andrews, R., O'Rourke, C., Hodgen, S., & Mills, A. (2021). Photocatalytic air purification: Effect of HNO<sub>3</sub> accumulation on NO<sub>x</sub> and VOC removal. *Catalysis Today*, 380, 105–113.
  10. Liu, Z., Zhang, X., Nishimoto, S., Murakami, T., & Fujishima, A. (2008). Efficient photocatalytic degradation of gaseous acetaldehyde by highly ordered TiO<sub>2</sub> nanotube arrays. *Environmental Science & Technology*, 42, 8547–8551.
  11. Moulis, F., & Krýsa, J. (2013). Photocatalytic degradation of several VOCs (*n*-hexane, *n*-butyl acetate and toluene) on TiO<sub>2</sub> layer in a closed-loop reactor. *Catalysis Today*, 209, 153–158.
  12. Ohtani, B., Prieto-Mahaney, O. O., Li, D., & Abe, R. (2010). What is Degussa (Evonik) P25? Crystalline composition analysis, reconstruction from isolated pure particles and photocatalytic activity test. *Journal of Photochemistry and Photobiology A: Chemistry*, 216, 179–182.
  13. Zita, J., Krýsa, J., & Mills, A. (2009). Correlation of oxidative and reductive dye bleaching on TiO<sub>2</sub> photocatalyst films. *Journal of Photochemistry and Photobiology A: Chemistry*, 203, 119–124.
  14. Zouzelka, R., Remzova, M., Brabec, L., & Rathousky, J. (2018). Photocatalytic performance of porous TiO<sub>2</sub> layers prepared by quantitative electrophoretic deposition from organic solvents. *Applied Catalysis B: Environmental*, 227, 70–78.
  15. Krýsa, J., Keppert, M., Waldner, G., & Jirkovský, J. (2005). Immobilized particulate TiO<sub>2</sub> photocatalysts for degradation of organic pollutants: Effect of layer thickness. *Electrochimica Acta*, 50, 5255–5260.
  16. Zlámál, M., Krýsa, J., & Jirkovský, J. (2009). Photocatalytic degradation of acid orange 7 on TiO<sub>2</sub> films prepared from various powder catalysts. *Catalysis Letters*, 133, 160.
  17. Huang, Y., Ho, S. S. H., Lu, Y., Niu, R., Xu, L., Cao, J., & Lee, S. (2016). Removal of indoor volatile organic compounds via photocatalytic oxidation: A short review and prospect. *Molecules*, 21, 56.
  18. Wang, S., Ang, H. M., & Tade, M. O. (2007). Volatile organic compounds in indoor environment and photocatalytic oxidation: State of the art. *Environment International*, 33, 694–705.
  19. Zhang, Y., Yang, R., & Zhao, R. (2003). A model for analyzing the performance of photocatalytic air cleaner in removing volatile organic compounds. *Atmospheric Environment*, 37, 3395–3399.
  20. Yang, L., Liu, Z., Shi, J., Hu, H., & Shangguan, W. (2007). Design consideration of photocatalytic oxidation reactors using TiO<sub>2</sub>-coated foam nickels for degrading indoor gaseous formaldehyde. *Catalysis Today*, 126, 359–368.
  21. Khalilzadeh, A., & Fatemi, S. (2016). Spouted bed reactor for VOC removal by modified nano-TiO<sub>2</sub> photocatalytic particles. *Chemical Engineering Research and Design*, 115, 241–250.
  22. Zhong, L., Haghighat, F., Lee, C.-S., & Lakdawala, N. (2013). Performance of ultraviolet photocatalytic oxidation for indoor air applications: Systematic experimental evaluation. *Journal of Hazardous Materials*, 261, 130–138.
  23. Shayegan, Z., Lee, C.-S., & Haghighat, F. (2018). TiO<sub>2</sub> photocatalyst for removal of volatile organic compounds in gas phase—A review. *Chemical Engineering Journal*, 334, 2408–2439.
  24. Guo, T., Bai, Z., Wu, C., & Zhu, T. (2008). Influence of relative humidity on the photocatalytic oxidation (PCO) of toluene by TiO<sub>2</sub> loaded on activated carbon fibers: PCO rate and intermediates accumulation. *Applied Catalysis B: Environmental*, 79, 171–178.
  25. Zhu, X., Chang, D.-L., Li, X.-S., Sun, Z.-G., Deng, X.-Q., & Zhu, A.-M. (2015). Inherent rate constants and humidity impact factors of anatase TiO<sub>2</sub> film in photocatalytic removal of formaldehyde from air. *Chemical Engineering Journal*, 279, 897–903.
  26. Maggos, T., Bartzis, J. G., Liakou, M., & Gobin, C. (2007). Photocatalytic degradation of NO<sub>x</sub> gases using TiO<sub>2</sub>-containing paint: A real scale study. *Journal of Hazardous Materials*, 146, 668–673.
  27. Moussiopoulos, N., Barmpas, P., Ossonlis, I., & Bartzis, J. (2008). Comparison of numerical and experimental results for the evaluation of the depollution effectiveness of photocatalytic coverings in street canyons. *Environmental Modeling and Assessment*, 13, 357–368.
  28. Boningari, T., Inturi, S. N. R., Suidan, M., & Smirniotis, P. G. (2018). Novel one-step synthesis of sulfur doped-TiO<sub>2</sub> by flame spray pyrolysis for visible light photocatalytic degradation of acetaldehyde. *Chemical Engineering Journal*, 339, 249–258.
  29. Hu, H., Xiao, W.-J., Yuan, J., Shi, J.-W., Chen, M.-X., & Shang Guan, W.-F. (2007). Preparations of TiO<sub>2</sub> film coated on foam nickel substrate by sol-gel processes and its photocatalytic activity for degradation of acetaldehyde. *Journal of Environmental Sciences*, 19, 80–85.
  30. Sopyan, I. (2007). Kinetic analysis on photocatalytic degradation of gaseous acetaldehyde, ammonia and hydrogen sulfide on nanosized porous TiO<sub>2</sub> films. *Science and Technology of Advanced Materials*, 8, 33–39.
  31. Wang, C., Rao, Z., Mahmood, A., Wang, X., Wang, Y., Xie, X., & Sun, J. (2021). Improved photocatalytic oxidation performance of gaseous acetaldehyde by ternary g-C<sub>3</sub>N<sub>4</sub>/Ag-TiO<sub>2</sub> composites under visible light. *Journal of Colloid and Interface Science*, 602, 699–711.
  32. Bianchi, C. L., Gatto, S., Pirola, C., Naldoni, A., Di Michele, A., Cerrato, G., Crocellà, V., & Capucci, V. (2014). Photocatalytic degradation of acetone, acetaldehyde and toluene in gas-phase: Comparison between nano and micro-sized TiO<sub>2</sub>. *Applied Catalysis B: Environmental*, 146, 123–130.
  33. Jung, S.-C., Kim, S.-J., Imaishi, N., & Cho, Y.-I. (2005). Effect of TiO<sub>2</sub> thin film thickness and specific surface area by low-pressure metal-organic chemical vapor deposition on photocatalytic activities. *Applied Catalysis B: Environmental*, 55, 253–257.
  34. Krýsa, J., Keppert, M., Jirkovský, J. R., Štengl, V., & Šubrt, J. (2004). The effect of thermal treatment on the properties of TiO<sub>2</sub> photocatalyst. *Materials Chemistry and Physics*, 86, 333–339.
  35. Sopha, H., Baudys, M., Hromadko, L., Lhotka, M., Pavlinak, D., Krysa, J., & Macak, J. M. (2022). Scaling up anodic TiO<sub>2</sub> nanotube layers—Influence of the nanotube layer thickness on the photocatalytic degradation of hexane and benzene. *Applied Materials Today*, 29, 101567.
  36. Stucchi, M., Galli, F., Bianchi, C. L., Pirola, C., Boffito, D. C., Biasioli, F., & Capucci, V. (2018). Simultaneous photodegradation of VOC mixture by TiO<sub>2</sub> powders. *Chemosphere*, 193, 198–206.
  37. Macak, J. M., Zlamal, M., Krysa, J., & Schmuki, P. (2007). Self-organized TiO<sub>2</sub> nanotube layers as highly efficient photocatalysts. *Small (Weinheim an der Bergstrasse, Germany)*, 3, 300–304.
  38. Zita, J., Krýsa, J., Černigoj, U., Lavrenčič-Štangar, U., Jirkovský, J., & Rathouský, J. (2011). Photocatalytic properties of different TiO<sub>2</sub> thin films of various porosity and titania loading. *Catalysis Today*, 161, 29–34.
  39. ISO 22197-2 Fine Ceramics, Advanced Technical Ceramics—Test Method for Air-Purification Performance of

- Semiconducting Photocatalytic Materials—Part 2: Removal of Acetaldehyde ISO, Geneva (2011).
40. Herrmann, J.-M. (2005). Heterogeneous photocatalysis: state of the art and present applications In honor of Pr. RL Burwell Jr. (1912–2003), Former Head of Ipatieff Laboratories, Northwestern University, Evanston (Ill). *Topics in catalysis*, *34*, 49–65.
  41. Krýsa, J., Baudys, M., & Mills, A. (2015). Quantum yield measurements for the photocatalytic oxidation of acid orange 7 (AO7) and reduction of 2,6-dichlorindophenol (DCIP) on transparent TiO<sub>2</sub> films of various thickness. *Catalysis Today*, *240*, 132–137.
  42. Krýsa, J., Baudys, M., Zlámal, M., Krýsová, H., Morozová, M., & Klusoň, P. (2014). Photocatalytic and photoelectrochemical properties of sol–gel TiO<sub>2</sub> films of controlled thickness and porosity. *Catalysis Today*, *230*, 2–7.
  43. Kartheuser, B., Costarramone, N., Pigot, T., & Lacombe, S. (2012). NORMACAT project: Normalized closed chamber tests for evaluation of photocatalytic VOC treatment in indoor air and formaldehyde determination. *Environmental Science and Pollution Research*, *19*, 3763–3771.
  44. Clough, S. R. (2014). Heptane. In P. Wexler (Ed.), *Encyclopedia of Toxicology (Third Edition)* (pp. 845–847). Academic Press.
  45. Saucedo-Lucero, J. O., & Arriaga, S. (2013). Photocatalytic degradation of hexane vapors in batch and continuous systems using impregnated ZnO nanoparticles. *Chemical Engineering Journal*, *218*, 358–367.

## Authors and Affiliations

Michal Baudys<sup>1</sup>  · Eleonore Berthet<sup>1</sup> · Jan M. Macak<sup>2,3</sup>  · Miloslav Lhotka<sup>1</sup> · Josef Krýsa<sup>1</sup> 

✉ Josef Krýsa  
krysaj@vscht.cz

<sup>1</sup> Department of Inorganic Technology, University of Chemistry and Technology Prague, Prague, Czech Republic

<sup>2</sup> Center of Materials and Nanotechnologies, University of Pardubice, Pardubice, Czech Republic

<sup>3</sup> Central European Institute of Technology, Brno University of Technology, Brno, Czech Republic